Coherent neuronal dynamics driven by optogenetic stimulation in the primate brain

Ryan A. Shewcraft[1], Heather L. Dean[2], Yan T. Wong[3,4,5], Maureen A. Hagan[4,5,6], Margaret M. Fabiszak[7] and Bijan Pesaran[1,8,9,*]

Lead Contact:
Bijan Pesaran, Ph.D.
4 Washington Pl. Rm 809
Center for Neural Science
New York University
New York, NY 10003 USA
Tel: 212.998.3578, Fax 212.995.4011
E-mail: bijan@nyu.edu

Word counts

Summary	139	(<150)
Introduction	537	
Results	2219	
Discussion	1301	
Experimental Procedures	415	
References	59	
Figures	7	
Tables	0	
Total words	4176	(< 4500)

[1]Center for Neural Science; New York University; New York, NY, 10003; United States
[2]Center for Neural Science; New York University; New York, NY, 10003, United States
[3] Department of Electrical and Computer Systems Engineering; Monash University; Clayton, VIC 3800; Australia
[4] Department of Physiology; Monash University; Clayton, VIC 3800; Australia
[5] Biomedicine Discovery Institute; Monash University; Clayton, VIC 3800; Australia
[6] Australian Research Council, Centre of Excellence for Integrative Brain Function; Monash University; Clayton, VIC 3800; Australia
[7] Laboratory of Neural Systems; The Rockefeller University; New York, NY, 10065; United States
[8] NYU Neuroscience Institute; New York University Langone Health; New York, NY, 10016; United States
[9] Lead Contact
[*] Correspondence: bijan@nyu.edu

Summary

Optogenetic stimulation offers powerful new ways to test the functional significance of coherent neuronal activity. In rodents, optogenetically stimulating specific classes of neurons has been shown to selectively perturb coherent neuronal dynamics. Testing the causal role of coherent neuronal dynamics for complex cognitive functions requires studies in non-human primates (NHP). How to selectively manipulate coherent dynamics in NHP, however, remains unclear due to lack of reliable cell-type expression. Here, we investigate neuronal dynamics in macaque frontal cortex when optogenetically stimulating neurons that express ChR2(H134R) pan-neuronally. Neuronal responses to optogenetic stimulation occurred within an effective temporal window of excitation that varied non-linearly with stimulation parameters. Given the observed temporal window of excitation, we designed model-based stimulation sequences to selectively perturb coherent dynamics. The results provide a procedure for using optogenetic stimulation to test the role of coherent neuronal dynamics for complex cognitive functions.

Introduction

Neuronal dynamics contain coherent temporal structure across a range of frequencies[1]. The term coherent neuronal dynamics describes fluctuations within specific temporal frequency bands that are revealed by correlating the time of spiking events to local field potentials (LFPs) using spike-field coherence[2]. In the primate brain, coherent neuronal dynamics have been implicated in the control of a range of higher cognitive functions including working memory[3–5], decision making[6–8], coordination[9,10], attention[11,12], and perception[13,14]. To go further and test the extent to which coherent neuronal dynamics are necessary and sufficient for complex cognitive functions requires causal manipulations that can selectively perturb temporal patterns of neuronal activity.

Electrical and magnetic stimulation approaches have been used to precisely generate temporal structure in neuronal activity[15–17] and study the impact of temporally patterned stimulation on behavior[18,19]. A significant difficulty in interpreting the results of causal manipulations, however, is that stimulating neuronal networks can lead to a variety of non-linear and dynamic response properties in addition to coherent dynamics[20–22]. Consequently, simultaneous recordings of neuronal activity during stimulation are needed to confirm the impact of stimulation sequences on coherent neuronal dynamics. Sequences of electrical and magnetic stimulation pulses can generate substantial recording artifacts that are difficult to suppress, especially for field potentials, obscuring responses and introducing significant confounds[23,24].

Optogenetic stimulation can generate temporally-precise patterns of activity in neuronal populations defined for manipulation through genetic modifications[25,26]. Unlike electrical or magnetic stimulation, light-based stimulation can be used in a manner that introduces few if any artifacts to simultaneous electrophysiological recordings. Optogenetic stimulation has great potential to selectively generate neuronal dynamics[27,28] and optogenetic stimulation of the

primate brain can perturb behavioral processes[29–31]. Previous work has emphasized that the formation and maintenance of coherent neuronal activity depends on the selective control of interneurons[28,32]. However, this work has been done in rodents, which reliably express optogenetic constructs in cell-type specific manner. Whether virally-mediated optogenetic stimulation in the NHP can test the causal role of neuronal dynamics in computation and behavior has not been systematically examined.

Here, we address the problem of how to generate coherent neuronal dynamics without expressing optogenetic constructs in a cell-type specific manner. We start by developing a model for coherent neuronal dynamics. According to the model, the frequency of coherent activity depends shaping excitation and inhibition to yield an effective response window – the E-I window. The model predicts that sequences of optogenetic stimulation pulses can be designed to shape synaptic excitation and inhibition and generate the desired coherent activity without cell-type specific expression. We then did experiments to test the model predictions. We expressed ChR2(H134R) pan-neuronally in macaque cortex, using a synapsin promoter delivered by an AAV2/5 viral injection, and measured spiking and local field potential (LFP) responses to optogenetic stimulation. To alter the E-I window, we stimulated across a range of stimulation sequences with different pulse rates and pulse durations. The results demonstrate that coherent dynamics can be generated across a wide range of frequencies consistent with the E-I window model. We conclude by presenting an experimental protocol for designing stimulation sequences that manipulate coherent neuronal dynamics. The resulting method provides a path to testing the causal role of coherent neuronal dynamics in computation and behavior following expression of a pan-neuronal promoter.

Results

Modeling stimulation-evoked coherent neuronal dynamics

We define neuronal coherence as spiking that occurs coherently with simultaneously-recorded LFP activity. When the spike times of a neuron can be predicted from fluctuations in LFP activity at a particular frequency, the spiking is said to be coherent at that frequency. Thus, neuronal coherence is defined by coherent spiking and LFP activity and can be measured by estimating spike-field coherence between spiking and nearby LFP activity[2,3].

Figure 1 presents a model of stimulation-evoked coherent neuronal dynamics. We model neuronal spiking according to a conditional intensity function[33]. In the absence of optogenetic stimulation, we model background spiking activity as a Poisson process with a constant rate, λ_0 (**Fig. 1A**). We model background LFP activity as a process with increased power at low frequencies–"brown noise". For simplicity, we further assume that background LFP activity is uncorrelated with spiking activity.

Optogenetic stimulation drives spiking and LFP responses. More specifically, optogenetic stimulation light pulses incident on a population of transduced neurons expressing ChR2 depolarize the transduced neurons within the illuminated stimulation zone. Direct activation of the transduced neurons leads to excitatory and inhibitory synaptic currents within the local network of neurons. The resulting currents alter when neurons fire spikes in response to stimulation. Excitatory currents lead neurons to fire spikes more frequently. Inhibitory currents lead neurons to fire spikes less frequently. The impact of optogenetic stimulation on spiking can, therefore, be modeled in terms of changes in spiking probability in the conditional intensity function. Since we do not have access to the intracellular conductance changes in response to each stimulation pulse, we model the impact of each optogenetic stimulation pulse by excitatory and inhibitory modulations in the probability of spiking, an excitation-inhibition (E-I) window.

We model LFP activity in response to optogenetic stimulation as a linear sum of background activity and activity due to each stimulation pulse (**Fig. 1B**). LFP activity predominantly reflects summed post-synaptic potentials[2,34]. Therefore, we model the driven component of LFP activity in terms of the net E-I response following each stimulation pulse.

We term this model of neuronal coherence the **E-I window model.** Since we model spontaneous spiking and LFP as uncorrelated, baseline activity does not contain SFC (**Fig. 1C**). Since optogenetic stimulation evokes changes in spike probability and LFP responses, this coupling means that the stimulation evokes spikes that are coherent with LFP activity and the coherence is due to the temporal dynamics, or "shape", of the E-I windows. (**Fig. 1D**). Therefore, according to the E-I window model, the frequency of coherent neuronal dynamics determined by the E-I window.

Note that the neuronal coherence described by the E-I window model depends on predictability between spikes and LFP activity which is measured by spike-field coherence. This construction is consistent with but does not require invoking an oscillator or other phase-consistent process.

Selectively generating coherent neuronal dynamics

According to the E-I window model, selectively changing the duration of the excitatory and inhibitory components of the E-I window should affect the frequency content of the driven coherent neuronal dynamics (**Fig. 2A,B**). We tested this prediction computationally. We modelled E-I windows as a weighted sum of excitatory and inhibitory components

$$EI = \beta_{exc} exc - \beta_{inh} inh$$

$$exc = Ae^{-At}\left(\frac{(At)^{\alpha_{exc}}}{\alpha_{exc}!}\right)$$

$$inh = Ae^{-At}\left(\frac{(At)^{\alpha_{inh}}}{\alpha_{inh}!}\right)$$

where α_{exc} and α_{inh} govern the temporal dynamics of the excitatory and inhibitory components, respectively (**Fig. 2C**). To test the effect of different E-I window dynamics on coherence, we simulated SFC while sweeping through values for the α_{exc} and α_{inh} parameters. Using both excitatory and inhibitory components provided a wide range of driven dynamics, suggesting that the interaction between excitation and inhibition may allow for generating selective dynamics across a wider range of frequencies (**Fig. 2F**). Additional computational work suggested that the interplay of E- and I-windows was important to this result (**Supplementary Fig. 1**). Taken together, these simulation results suggest that coherent neuronal dynamics can be selectively generated using optogenetic stimulation to control E-I window durations, consistent with the E-I window model.

Optogenetic stimulation robustly generates frequency-selective responses

To test the E-I window model, we studied how pan-neuronally mediated optogenetic stimulation can be used to selectively generate coherent neuronal dynamics. We injected AAV5-hSyn-ChR2(H134R)-EYFP and recorded neuronal responses in three macaque monkeys (the inferior and superior parietal lobules in Monkeys H and J and lateral to the post-central dimple in Monkey B; **Fig. 3A).** We observed strong viral expression at each injection site with robust labelling of neurons and neuropil (**Fig. 3B**). *In vivo* optogenetic stimulation consisted of one second long sequences of light pulses (stimulation epoch) followed by 1-3 s of no stimulation (baseline epoch) (**Fig. 3C**). Optogenetic stimulation reliably generated neural responses. These

responses consisted of action potentials as well as large evoked field potentials visible on an individual pulse basis in the raw data (**Fig. 3D,E,F).**

We then measured neuronal responses to stimulation sequences composed of periodic and Poisson pulse trains with different pulse rates and pulse durations. **Figure 4A** presents example neuronal responses during a stimulation block with 5 ms wide pulses delivered with a 20 pulse/s Poisson pulse train. Individual stimulation pulses drove spiking activity and evoked LFP responses at the stimulation site (**Fig. 4Ai,ii**). Stimulation drove spiking activity that was coherent with LFP activity at selective frequencies (**Fig. 4Aiii**). To quantify the response to the pulse train, we computed the power spectrum of LFP activity during the one second long stimulation period (**Fig. 4Aiv**). The peri-stimulation LFP power spectrum revealed a significant increase in power (Chi-squared test, $p<0.01$).

We defined a power spectral ratio (PSR) as the ratio of the driven response to the baseline response and measured increases in power that extended throughout the entire stimulation sequence (**Fig. 4Av,vi**). This measure captures the linearly-dependent influence of optogenetic stimulation on temporal structure in the neuronal activity (see **Methods**). The PSR reveals the frequency selective increase in driven coherent neuronal activity as measured by LFP activity. Since driven spiking activity was not measured at all recording sites across the population, LFP activity provided a robust indicator of the driven coherent dynamics.

Longer pulse durations generated longer duration changes in firing rate (**Fig. 4B**). Interestingly, LFP activity during wider pulses showed longer periods of excitation and inhibition and this was associated with more selective changes in SFC and LFP power spectrum. Therefore, stimulation sequences with different pulse durations can be used to selectively generate coherent neuronal dynamics, consistent with changing the E-I window duration. Thus,

the E-I window model predicted the relationship between the E-I windows and the stimulation-evoked coherent neuronal dynamics.

Optogenetic stimulation generates pulse duration dependent responses

We averaged SFC across a population of recording sites with driven spiking activity in response to stimulation using Poisson pulse trains with 5, 10, 15, and 20 ms duration pulses (see **Methods**). SFC varied with pulse duration, consistent with the example site (**Fig. 4C**). In addition, we analyzed LFP responses across recording sites with driven evoked potentials in the three animals for 2, 5, 8, 10, 12, 15, 18, and 20 ms duration pulses. As with the example site, the frequency content of the driven LFP varied with pulse duration across the population (**Fig. 4C**).

To identify the frequency for which driven coherent activity was greatest, we fit the average SFC for each pulse with a polynomial (degree = 4) and identified the peak location. The frequency at which the maximal driven coherence decreased with pulse duration (r^2 = 0.88, p = 0.062) (**Fig. 4C**, red). For each stimulation condition at each recording site with evoked LFP responses, we summarized the PSR as a sum of Gaussians. Consistent with the SFC, the peak of the driven LFP, measured by the location of the peak of the first Gaussian, was dependent on pulse duration (r^2 = 0.602, p = 6.7×10^{-9}) (**Fig. 4C**, black). Longer duration pulses generated increases in coherent neuronal activity at lower frequencies. The center frequency of the driven responses did not depend on the mean pulse rate for Poisson stimulation (**Supplementary Fig. 2**). These results show that the selectivity and specificity of coherent neuronal dynamics generated by patterned stimulation depends on the temporal window of excitation in a manner that is consistent across cortical regions.

Site specific E-I window generation

Observed E-I windows may differ across stimulation parameters or across stimulation sites with different patterns of transfection and network connections (**Fig. 5A**). Within a single stimulation site, different pulse durations generate different frequency structure of the coherent neuronal activity, as predicted by the E-I window model (**Fig. 5B,C**). Using a shorter pulse generates a narrower response in LFP activity. In the model, the corresponding E-I window has narrower excitatory and inhibitory components than for longer pulses. Using this E-I window in the model results in broader coherence with a peak at higher frequencies compared to the longer pulse. Additionally, at a different, nearby injection site or in a different subject, the ChR2 expression pattern may differ. The observed E-I window may differ depending on how activity is recruited due to the specific expression pattern and local synaptic connectivity (**Fig. 5D**). A short pulse at Site B drives a narrower response in LFP activity, similar to Fig. 5C. However, in this case there is less overlap between excitatory and inhibitory components. As a result, stimulation with the same parameters at a different site can result in a different interaction between excitatory and inhibitory components in the network and hence different coherent neuronal dynamics.

These results indicate that 1 - variability is present in the shape of the stimulation-evoked E-I window; 2 - different coherent neuronal dynamics can be driven at different cortical sites for the same stimulation parameters; and 3 - optogenetic stimulation parameters need to be selected for each stimulation site to generate the desired neuronal coherence.

Model-based characterization of local response dynamics

In order to generalize stimulation parameters for selective generation given variability across response sites, we used the empirically measured E-I response for one pulse duration in the model to predict responses for other pulse durations. To do this, we temporally scaled the E-

I response for a 10 ms pulse to provide an estimate of the temporal window of excitation to any arbitrary pulse duration (**Fig. 6A**). Scaling longer pulse durations, which have excitation windows that capture high frequency suppression, provides a better fit to experimental data than scaling shorter pulses (**Supplementary Fig. S3**). Performing simulations in the model with E-I windows that are temporally scaled versions of the experimental test condition produces a map that shows which frequencies can be generated using pulsatile Poisson stimulation (**Fig. 6B**). The E-I window model generates dynamics that match empirical results (**Fig. 6B**, black dots). Importantly, different pulse durations can be used to generate selective responses in bands typically associated with alpha, beta, low-gamma, and high-gamma frequencies (**Fig. 6C**). This offers a way to separately test the contribution of each of these frequency bands to behavior.

Model-based prediction of responses to other forms of stimulation

The presence of site-dependent stimulation responses substantially complicates the task of selecting the stimulation parameters to selectively generate particular coherent neuronal dynamics. If the E-I window model could be used to predict responses to arbitrary stimulation pulse sequences, manipulating neuronal coherence would be experimentally less complex. Here we consider one such generalization**:** a quasi-periodic stimulation pulse train where the probability of generating a stimulation pulse is given by $P(stim) = \beta(1 + \alpha \sin(2\pi F t))\Delta t$ (**Fig. 7A**). Periodic stimulation can be used to generate frequency selective responses. However, response linearity means responses to periodic stimulation trains have power at the fundamental frequency and its harmonics, especially at low frequencies (**Fig. 7B**). Quasi-periodic stimulation can reduce the stimulation harmonic content, while preserving the response at the frequency of interest leading to selective drive (**Fig. 7C**). The quasi-periodic algorithm does not deliver stimulation pulses on regular intervals. Although frequency-selective drive is present on average across many trials, quasi-periodic stimulation may not reliably drive selective increases in power on individual trials with a small number of cycles. However,

frequency specificity is also present on a trial-by-trial basis (**Fig. 7D**). Therefore, a quasi-periodic algorithm can generate frequency selective drive over short, behaviorally relevant periods of time.

Quasi-periodic stimulation offers other benefits. With periodic stimulation, increasing stimulation intensity by stimulating more frequently can also increase the frequency of driven responses. By varying the modulation depth, α, of stimulation, quasi-periodic stimulation allows frequency-selective stimulation intensity to be controlled separately from the frequency of interest itself. Increasing α increases the number of stimulation pulses added preferentially at intervals around the period of the frequency of interest. This results in greater responses around the frequency of interest and not at other frequencies (**Fig. 7E**). Changing the frequency of interest is achieved by varying F in order to generate a range of behaviorally relevant frequencies (**Fig. 7F, Supplementary Fig. 4**).

One concern highlighted by our results is that responses to square wave pulse trains have low power at nodes determined by the inverse of the pulse duration. Since response linearity predicts that responses are shaped by the pulse shape, if the pulse shape has low power at a given frequency, then a periodic or quasi-periodic pulse train will not drive responses at that frequency (**Fig. 7F**, green). Conversely, if the pulse shape has a peak in power at a given frequency, then the response will be greater compared to stimulation at other desired frequencies with the same pulse duration (**Fig. 7F).** To address this concern, the pulse duration should be chosen according to the desired response frequency (**Fig. 7G**).

Discussion

Here, we used a model of spiking an LFP activity to parameterize optogenetic stimulation-evoked neuronal coherence in macaque cortex. We found that optogenetic stimulation generated selective coherent neuronal dynamics consistent with recruitment of excitatory and inhibitory activity. Using Poisson pulse trains, we varied pulse duration and pulse rate to characterize the coherent neuronal dynamics during stimulation. Our experimental results show that varying the pulse duration selectively alters driven coherence. Modeling results revealed that neuronal coherence can result from a combination of recruitment of excitatory and inhibitory responses in the network. Taken together, these results demonstrate how optogenetic stimulation in macaque cortex can be parametrically varied to selectively generate coherent dynamics across a range of behaviorally relevant frequencies (20-50 Hz) without necessarily targeting optogenetic stimulation to particular neuronal cell types.

Pan-neuronal stimulation and mechanisms of neuronal coherence

Previous work has used cell-type-specific optogenetic stimulation to generate coherent neuronal dynamics and study the effect of perturbing specific cell types on neuronal activity[27,32,35]. Direct stimulation of specific types of neurons recruits synaptically-mediated responses from other neurons in the network[36]. This recruited network activity shapes the frequency content of coherent neuronal dynamics[37]. Thus, stimulation-evoked coherence measured under cell-type-specific optogenetic stimulation can also reflect activity across a range of cell-types. Thus, although pan-neuronal optogenetic stimulation directly activates a heterogeneous range of cell types, stimulation-evoked coherence measured under pan-neuronal optogenetic stimulation may reflect stimulation-evoked coherence under cell-type-specific stimulation, albeit by activating network activity differently.

Parametric control for studying coherent neuronal dynamics during behavior

Continuous stimulation and pulsatile stimulation have been used to generate frequency specific dynamics in order to study their effects on behavior[27,32,35,38]. However, for continuous stimulation, the frequency range of generated coherent neuronal dynamics depends on local network properties, typically resulting in increased gamma activity[27] due interactions between excitatory and inhibitory neurons[39] that may vary in peak frequency across subjects[38]. Additionally, pulsatile stimulation of specific cell-types may not be able to generate a range of frequencies despite changes in stimulation parameters[28]. As well as gamma frequencies, coherent neuronal dynamics in theta[40,41], alpha[42,43] and beta[10,44] bands have been shown to play a role in neuronal computation and behavior. Studying the behavioral effects of dynamics in these frequency bands with causal manipulations may require additional stimulation strategies that allow for greater parametric control. Here we show that with pan-neuronal ChR2 expression, frequency selectivity can be achieved by varying stimulation sequence parameters to create excitation windows that generate coherent neuronal dynamics across a range of frequencies. Therefore, it is possible that pan-neuronal pulsatile stimulation with targeted parameter selection can be used to generate frequency selective coherent neuronal dynamics across a wider range of behaviorally-relevant frequencies than cell-type specific approaches.

Model-based selection of parameters

The coherent response dynamics we observed are likely due to the generation of varied excitation windows through the choice of pulse duration. As pulse duration increased, the peak response frequency fell (see **Fig. 4E**). However, the frequency structure of the driven dynamics varied slightly by site, which was likely due to local variations in ChR2 expression and network properties. Importantly, this suggests that in order to generate response in a frequency band of interest, the stimulus pulse train needs to be designed while taking into account the local

network properties. Stimulation triggered evoked LFPs reveal the temporal structure of windows of excitation and inhibition[45,46], which may capture the underlying network properties. The E-I window model uses response windows derived from experimentally measured evoked potentials and thus potentially accounts for intrinsic dynamics due to the local network. Using empirically-derived responses from one set of parameters in the E-I window model to estimate responses to other parameters allows for model-based, site-specific selection of pulsatile stimulation parameters. Additionally, the E-I window model may be useful because it allows alternative stimulation sequence designs to be optimized. For example, generating coherent dynamics may also be possible with shorter pulses using different opsins that have slower dynamics[47], or using non-pulse-based stimulation dynamics[48]. The E-I window model could be used to predict coherent neuronal dynamics that arise from alternative forms of stimulation to aid in selection of opsin type and stimulation parameters for novel paradigms.

Coherent dynamics result from linking mechanisms generating spiking and LFP

LFP activity arises from synchronous neuronal activity that occurs due to temporally structured fluctuations of local excitation and inhibition[39,49,50]. Increases in LFP power may indicate either an overall increase in neuronal activity or an increase in temporally-structured activity[2]. However, if the mechanism which generates spiking is not coupled with the mechanism that generates LFP activity, then there will be no SFC. We found that optogenetic stimulation drove spiking activity that was coherent with LFP activity and was consistent with the stimulation-induced LFP power changes. This suggests that optogenetic stimulation provides a common input that couples spiking and LFP activity. Therefore, LFP responses generated by optogenetic stimulation are at least in part due to increases in temporally-structured, coherent neuronal activity resulting from parametric generation of windows of excitation and inhibition.

Due to the biophysics of extracellular potentials, LFP activity is most sensitive to postsynaptic potentials in neurons where the positive and negative current sources are separated to provide an open field geometry[2]. Thus, contributions from neurons with extended dendritic architectures, such as pyramidal neurons, are more heavily weighted by LFP activity. Additionally, pyramidal neurons typically have larger cell bodies than other cortical neurons and thus have more easily measurable actions potentials. Therefore, our measurement of both spiking activity and LFP may be biased toward contributions from pyramidal neurons, thereby biasing our estimate of SFC toward the relationship between postsynaptic potentials and action potentials of spiking neurons. Novel recording technologies that offer measurements of intra-cellular potentials simultaneously across a large population of neurons may be necessary to explore the contribution of neurons with closed-field geometries.

Mechanisms of frequency selectivity

How do longer pulses, with increased excitation, shift coherent dynamics toward lower frequencies? We propose that cell-type specific recruitment of inhibition may be enhanced by greater excitation from longer duration pulses. Mammalian neo-cortex contains many interneuron sub-types[51,52] which may play distinct roles in cortical computations[53,54]. Following stimulation, excitation may recruit interneuron activity across a range of these cell types[39,55–57], but the somatostatin and PV+ subtypes likely play a preferential role in suppressing high frequency activity[28,32,58]. In particular, somatostatin interneurons that inhibit PV+ interneurons, could reduce gamma activity. If so, we predict that somatostatin interneurons may show an increase in firing rate after stimulation, and PV+ and excitatory neurons may decrease in firing rate due to the increased inhibition, particularly for longer pulses. The duration and degree of inhibition due to interneuron recruitment may also depend non-linearly on the duration and degree of network excitation. Additional work is needed to test this mechanism for shifts towards lower frequencies with loner duration excitatory windows. Recordings from identified excitatory

and inhibitory neurons are necessary to assess the network recruitment of inhibition at a cellular level. Performing this test depends on inhibitory cell-type specificity that is currently unavailable in primates but may be possible using novel genetic targeting strategies[31,59]. Alternatively, biophysical models of optogenetic stimulation in large-scale, heterogeneous neural networks may offer predictions about cell-type specific contributions to coherent neuronal dynamics.

In conclusion, we systematically studied neuronal responses to optogenetic stimulation in macaque frontal cortex. We highlight the role of designing Poisson, quasi-periodic, and other pulsatile stimulation sequences that generate temporal windows of excitation to recruit inhibition without necessarily targeting specific types of neurons. In general, our results show that combining experimental measures with model-based predictions can be used to study how optogenetic stimulation drives network dynamics across a wide range of experimental designs, including using different brain regions, model species, cell-type selectivity, and stimulation protocols. These results demonstrate that the ability to selectively generate dynamics in the primate brain can be useful for understanding how coherent neuronal dynamics give rise to behavior.

Online Methods:

Animals

Experiments were performed with two male rhesus macaques (*Macaca mulatta*) and one male cynomolgus macaque (*Macaca fascicularis*) All surgical and animal care procedures were approved by the New York University Animal Care and Use Committee and were performed in accordance with the National Institute of Health guidelines for care and use of laboratory animals.

Injection surgery

We performed injections of optogenetic viral vectors in two rhesus macaques (Monkeys H and J) and one cynomolgus macaque (Monkey B) 6-25 weeks prior to recording. One microliter of AAV5-hSyn-ChR2(h134R)-EYFP was injected through 26 s gauge stainless steel cannulas at a rate of 0.05 μl/min. We made injections at 2-3 depths spaced 500-750 μm across 2-4 sites per animal.

Optical Stimulation

Light power at the tip was measured prior to each experiment and varied from 16-20.5 mW. (510-653 mW/mm^2). The fiber optic was placed on top of a thinned dura. Stimulation sequences were controlled by custom LabVIEW (National Instruments) code.

Electrophysiology

We recorded responses from injection sites with successful transduction. We recorded neural signals from awake, alert subjects while they were seated, head-fixed in a primate chair in a dark, quiet room. Neural signals were recorded on glass-coated tungsten electrodes (Alpha-Omega, impedance: 0.8-1.2 MΩ at 1 kHz). The electrode was attached to a microdrive (Flex

MT, Alpha-Omega). We recorded driven multi-unit activity and LFP responses at one site in each animal, and driven LFP responses without driven multi-unit activity in an additional 4 sites across the subjects.

Fitting E-I Windows

E-I windows were fit to the form

$$EI = Ae^{-At}\left(\frac{\beta_{exc}(At)^{\alpha_{exc}}}{\alpha_{exc}!} - \frac{\beta_{inh}(At)^{\alpha_{inh}}}{\alpha_{inh}!}\right)$$

which has an excitatory and inhibitory component. The constraint $\alpha_{exc} < \alpha_{inh}$ was used in order to ensure that excitation precedes inhibition. For the pure simulations, A, β_{exc} and β_{inh} were set to 1. To fit empirical E-I windows, all parameters were fit using a grid search to minimize the squared error between the modelled window and the empirical window.

E-I Window Model

We modelled spiking activity that was coherent with LFP activity using a Poisson point process with a conditional intensity function. The instantaneous firing rate was modelled as

$$\lambda(t) = (\lambda_E(t) + \lambda_I(t) + \lambda_0)\cdot dt$$
$$\lambda_E(t) = f(E(t)) = e^{E(t)}$$
$$\lambda_I(t) = g(I(t)) = e^{I(t)}$$

where λ_0 is the baseline firing rate, dt is the sampling rate. $E(t)/I(t)$ is the time course of optogenetically driven E and I windows, respectively, that generates the fluctuations in the conditional intensity function. It is determined by convolving the E and I window with a Poisson process generated from the stimulus sequence parameters.

Analysis

Analysis was performed in MATLAB (The Mathworks). Spectral analysis was performed using multi-taper methods[60].

Additional details can be found in the **Supplemental Experimental Procedures**

Acknowledgements:

BRAIN R01-NS104923. R01-EY024067, P30-EY013079, T32-EY007136, a Scholar Award from the McKnight Endowment Fund for Neuroscience (BP) and an Alfred P Sloan Foundation.

Author Contributions:

Conceptualization: R.A.S., H.L.D., Y.T.W., M.A.H., and B.P.; Methodology: R.A.S., H.L.D., Y.T.W., M.A.H., M.F.F. and B.P.; Software: R.A.S., H.L.D., and B.P.; Formal Analysis: R.A.S. and B.P.; Investigation: R.A.S. and B.P.; Resources: R.A.S., H.L.D., and B.P.; Writing – Original Draft: R.A.S. and B.P.; Writing – Review & Editing: R.A.S., H.L.D., Y.T.W., M.A.H., M.F.F. and B.P.; Visualization: R.A.S. and B.P.; Supervision: H.L.D., Y.T.W., M.A.H., and B.P.; Funding Acquisition: B.P.

Competing Financial Interests:

The authors declare no competing financial interests.

References

1. Buzsáki, G., Anastassiou, C. a. & Koch, C. The origin of extracellular fields and currents — EEG, ECoG, LFP and spikes. *Nat Rev Neurosci* **13,** 407–420 (2012).
2. Pesaran, B. *et al.* Investigating large-scale brain dynamics using field potential recordings: analysis and interpretation. *Nat. Neurosci.* (2018). doi:10.1038/s41593-018-0171-8
3. Pesaran, B., Pezaris, J. S., Sahani, M., Mitra, P. P. & Andersen, R. A. Temporal structure in neuronal activity during working memory in macaque parietal cortex. *Nat. Neurosci.* **5,** 805–811 (2002).
4. Salazar, R. F., Dotson, N. M., Bressler, S. L. & Gray, C. M. Content-Specific Fronto-Parietal Synchronization During Visual Working Memory. *Science (80-.).* **1097,** (2012).
5. Siegel, M., Warden, M. R. & Miller, E. K. Phase-dependent neuronal coding of objects in short-term memory. *Proc. Natl. Acad. Sci. U. S. A.* **106,** 21341–21346 (2009).
6. Pesaran, B., Nelson, M. J. & Andersen, R. A. Free choice activates a decision circuit between frontal and parietal cortex. *Nature* **453,** 406–409 (2008).
7. Hawellek, D. J., Wong, Y. T. & Pesaran, B. Temporal coding of reward-guided choice in the posterior parietal cortex. *Proc Natl Acad Sci USA* **113,** 13492–13497 (2016).
8. Wong, Y. T., Fabiszak, M. M., Novikov, Y., Daw, N. D. & Pesaran, B. Coherent neuronal ensembles are rapidly recruited when making a look-reach decision. *Nat Neurosci* **19,** 1–11 (2016).
9. Hagan, M. A., Dean, H. L. & Pesaran, B. Spike-field activity in parietal area LIP during coordinated reach and saccade movements. *J. Neurophysiol.* **107,** 1275–1290 (2012).
10. Dean, H. L., Hagan, M. A. & Pesaran, B. Only Coherent Spiking in Posterior Parietal Cortex Coordinates Looking and Reaching. *Neuron* **73,** 829–841 (2012).

11. Buschman, T. J. & Miller, E. K. Top-down versus bottom-up control of attention in the prefrontal and posterior parietal cortices. *Science* **315,** 1860–2 (2007).

12. Gregoriou, G. G., Gotts, S. J., Zhou, H. & Desimone, R. High-Frequency, Long-Range Coupling Between Prefrontal and Visual Cortex During Attention. **324,** 1207–1211 (2009).

13. Gray, C. M., König, P., Engel, A. K. & Singer, W. Oscillatory responses in cat visual cortex exhibit inter-columnar synchronization which reflects global stimulus properties. *Nature* **338,** 334–337 (1989).

14. Womelsdorf, T., Fries, P., Mitra, P. P. & Desimone, R. Gamma-band synchronization in visual cortex predicts speed of change detection. *Nature* **439,** 733–736 (2006).

15. Casarotto, S. *et al.* EEG responses to TMS are sensitive to changes in the perturbation parameters and repeatable over time. *PLoS One* **5,** (2010).

16. Radman, T., Su, Y., An, J. H., Parra, L. C. & Bikson, M. Spike timing amplifies the effect of electric fields on neurons: implications for endogenous field effects. *J. Neurosci.* **27,** 3030–6 (2007).

17. Schmidt, S. L., Iyengar, A. K., Foulser, A. A., Boyle, M. R. & Fr??hlich, F. Endogenous cortical oscillations constrain neuromodulation by weak electric fields. *Brain Stimul.* **7,** 878–889 (2014).

18. Bari, B. A., Ollerenshaw, D. R., Millard, D. C., Wang, Q. & Stanley, G. B. Behavioral and electrophysiological effects of cortical Microstimulation parameters. *PLoS One* **8,** 1–13 (2013).

19. Van Acker, G. M. *et al.* Effective intracortical microstimulation parameters applied to primary motor cortex for evoking forelimb movements to stable spatial end points. *J. Neurophysiol.* **110,** 1180–9 (2013).

20. Millard, D. C., Wang, Q., Gollnick, C. A. & Stanley, G. B. System identification of the nonlinear dynamics in the thalamocortical circuit in response to patterned thalamic microstimulation in vivo. *J. Neural Eng.* **10,** 066011 (2013).

21. Nassi, J. J., Avery, M. C., Cetin, A. H., Roe, A. W. & Reynolds, J. H. Optogenetic Activation of Normalization in Alert Macaque Visual Cortex. *Neuron* **86,** 1504–17 (2015).

22. Muldoon, S. F. *et al.* Stimulation-Based Control of Dynamic Brain Networks. *PLoS Comput. Biol.* **12,** (2016).

23. Olsson, R. H., Buhl, D. L., Sirota, A. M., Buzsaki, G. & Wise, K. D. Band-tunable and multiplexed integrated circuits for simultaneous recording and stimulation with microelectrode arrays. *IEEE Trans. Biomed. Eng.* **52,** 1303–11 (2005).

24. Mueller, J. K. *et al.* Simultaneous transcranial magnetic stimulation and single-neuron recording in alert non-human primates. *Nat. Publ. Gr.* **17,** 1130–1136 (2014).

25. Boyden, E. S., Zhang, F., Bamberg, E., Nagel, G. & Deisseroth, K. Millisecond-timescale, genetically targeted optical control of neural activity. *Nat. Neurosci.* **8,** 1263–8 (2005).

26. Han, X. *et al.* Millisecond-timescale optical control of neural dynamics in the nonhuman primate brain. *Neuron* **62,** 191–8 (2009).

27. Adesnik, H. & Scanziani, M. Lateral competition for cortical space by layer-specific horizontal circuits. *Nature* **464,** 1155–1160 (2010).

28. Cardin, J. a *et al.* Driving fast-spiking cells induces gamma rhythm and controls sensory responses. *Nature* **459,** 663–7 (2009).

29. Dai, J., Brooks, D. I. & Sheinberg, D. L. Optogenetic and electrical microstimulation systematically bias visuospatial choice in primates. *Curr. Biol.* **24,** 63–69 (2014).

30. Jazayeri, M., Lindbloom-Brown, Z. & Horwitz, G. D. Saccadic eye movements evoked by optogenetic activation of primate V1. *Nat. Neurosci.* **15,** 1368–1370 (2012).

31. Stauffer, W. R. *et al.* Dopamine Neuron-Specific Optogenetic Stimulation in Rhesus Macaques. *Cell* **166,** 1564–1571.e6 (2016).

32. Sohal, V. S., Zhang, F., Yizhar, O. & Deisseroth, K. Parvalbumin neurons and gamma rhythms enhance cortical circuit performance. *Nature* **459,** 698–702 (2009).

33. Brown, E. N., Barbieri, R., Eden, U. T. & Frank, L. M. in *Computational Neuroscience: A*

Comprehensive Approach (ed. Feng, J.) 253–286 (CRC Press, 2003).

34. Buzsáki, G., Anastassiou, C. a. & Koch, C. The origin of extracellular fields and currents — EEG, ECoG, LFP and spikes. *Nat. Rev. Neurosci.* **13,** 407–420 (2012).

35. Cardin, J. a *et al.* Driving fast-spiking cells induces gamma rhythm and controls sensory responses. *Nature* **459,** 663–667 (2009).

36. Phillips, E. A. K. & Hasenstaub, A. R. Asymmetric effects of activating and inactivating cortical interneurons. *Elife* **5,** 1–22 (2016).

37. Kato, H. K., Asinof, S. K. & Isaacson, J. S. Network-Level Control of Frequency Tuning in Auditory Cortex. *Neuron* **95,** 412–423.e4 (2017).

38. Ni, J. *et al.* Gamma-Rhythmic Gain Modulation. *Neuron* **92,** 240–251 (2016).

39. Buzsáki, G. & Wang, X.-J. Mechanisms of Gamma Oscillations. *Annu. Rev. Neurosci.* **35,** 203–225 (2012).

40. Lee, H. *et al.* Phase Locking of Single Neuron Activity to Theta Oscillations during Working Memory in Monkey Extrastriate Visual Cortex. **45,** 147–156 (2005).

41. Jutras, M. J., Fries, P. & Buffalo, E. a. Oscillatory activity in the monkey hippocampus during visual exploration and memory formation. *Proc. Natl. Acad. Sci.* **110,** 13144–13149 (2013).

42. Spaak, E., Bonnefond, M., Maier, A., Leopold, D. a. & Jensen, O. Layer-specific entrainment of gamma-band neural activity by the alpha rhythm in monkey visual cortex. *Curr. Biol.* **22,** 2313–2318 (2012).

43. Kerkoerle, T. Van, Self, M. W., Dagnino, B., Gariel-mathis, M. & Poort, J. Alpha and gamma oscillations characterize feedback and feedforward processing in monkey visual cortex. **111,** 14332–14341 (2014).

44. Haegens, S. *et al.* Beta oscillations in the monkey sensorimotor network reflect somatosensory decision making. *PNAS* 1–6 (2011). doi:10.1073/pnas.1107297108/-/DCSupplemental.www.pnas.org/cgi/doi/10.1073/pnas.1107297108

45. Poulet, J. F. A. & Petersen, C. C. H. Internal brain state regulates membrane potential synchrony in barrel cortex of behaving mice. *Nature* **454,** 881–885 (2008).

46. Okun, M., Naim, A. & Lampl, I. The Subthreshold Relation between Cortical Local Field Potential and Neuronal Firing Unveiled by Intracellular Recordings in Awake Rats. *J. Neurosci.* **30,** 4440–4448 (2010).

47. Berndt, A., Yizhar, O., Gunaydin, L. A., Hegemann, P. & Deisseroth, K. Bi-stable neural state switches. *Nat Neurosci* **12,** 229–34 (2009).

48. Tchumatchenko, T., Newman, J. P., Fong, M. & Potter, S. M. Delivery of continuously-varying stimuli using channelrhodopsin-2. *Front Neural Circuits* **7,** 184 (2013).

49. Csicsvari, J., Jamieson, B., Wise, K. D. & Buzsáki, G. Mechanisms of gamma oscillations in the hippocampus of the behaving rat. *Neuron* **37,** 311–322 (2003).

50. Hasenstaub, A. *et al.* Inhibitory postsynaptic potentials carry synchronized frequency information in active cortical networks. *Neuron* **47,** 423–435 (2005).

51. Wonders, C. P. & Anderson, S. A. The origin and specification of cortical interneurons. *Nat. Rev. Neurosci.* **7,** 687–696 (2006).

52. Markram, H. *et al.* Interneurons of the neocortical inhibitory system. *Nat. Rev. Neurosci.* **5,** 793–807 (2004).

53. Kepecs, A. & Fishell, G. Interneuron cell types are fit to function. *Nature* **505,** 318–326 (2014).

54. Roux, L. & Buzsáki, G. Tasks for inhibitory interneurons in intact brain circuits. *Neuropharmacology* **88,** 10–23 (2015).

55. Gloveli, T. *et al.* Differential involvement of oriens/pyramidale interneurones in hippocampal network oscillations in vitro. *J. Physiol.* **562,** 131–147 (2005).

56. Pike, F. G. *et al.* Distinct frequency preferences of different types of rat hippocampal neurones in response to oscillatory input currents. *J. Physiol.* **529,** 205–213 (2000).

57. Tukker, J. J., Fuentealba, P., Hartwich, K., Somogyi, P. & Klausberger, T. Cell Type-

Specific Tuning of Hippocampal Interneuron Firing during Gamma Oscillations In Vivo. *J. Neurosci.* **27,** 8184–8189 (2007).

58. Pfeffer, C. K., Xue, M., He, M., Huang, Z. J. & Scanziani, M. Inhibition of inhibition in visual cortex: the logic of connections between molecularly distinct interneurons. *Nat. Neurosci.* **16,** 1068–76 (2013).

59. Galvan, A. *et al.* Nonhuman Primate Optogenetics: Recent Advances and Future Directions. *J Neurosci* **37,** 10894–10903 (2017).

60. Mitra, P. P. & Pesaran, B. Analysis of dynamic brain imaging data. *Biophys. J.* **76,** 691–708 (1999).

Figure Legends

Figure 1. Excitation and inhibition drive coherent neuronal dynamics. (A) During spontaneous activity, synaptic inputs drive activity in a local network. We model spiking as being generated from a Poisson process with a constant rate and LFP as being generated from a Brown noise process. Under these assumptions, spontaneous spiking is not coherent with spontaneous LFP. **(B)** To model of optogenetic stimulation of a transfected, we simulated pulsatile responses generated by direct activation of ChR2 channels and synaptic activity. Pulsatile responses are convolved with a stimulation sequence. The summed excitatory and inhibitory (E-I, black) components comprise the simulated LFP. The individual E (blue) and I (red) windows, govern the variable spiking rate in the Poisson process which generates coherent spiking. **(C)** Spontaneous activity in the model has no spike-field coherence. (D) Optogenetic stimulation drives correlated fields and spiking, leading to frequency selective spike-field coherence.

Figure 2. E-I window shape controls frequency of coherent activity. (A) Idealized generation of frequency selective coherent neuronal dynamics. The frequency content of the coherent activity varies with stimulation parameters. **(B)** Example coherence for various stimulus parameters in (A). **(C)** Excitation, inhibition and E-I windows with varying parameters to alter the duration of the windows. E-I is the sum of E and I windows. **(D)** Spike-field coherence (left) and power spectral ratio (right) that result from using the E windows from (C) in the model. Right, frequency of peaks in the SFC (blue) and PSR (red) for each E window. **(E)** The same as (D) using I windows. **(F)** The same as (D) using E-I windows. **(G)** Differences in the peak frequencies for each window duration for E(black), I (yellow) and E-I (green) windows.

Figure 3. Optogenetic stimulation in macaque cortex. (A) Recording locations in all animals. The area of the circle corresponds to the number of sites recorded in each animal. **(B)** Example injection site with YFP labeled neurons and neuropil from horizontal section. *Inset*: image of a single transduced neuron. **(C)** Experimental design featured a 1 s stimulation pulse sequence followed by 1-3 s without stimulation. **(D)** Example raster plot (*top*) and PSTH (*bottom*) of the spiking response triggered on each stimulation pulse for Poisson distributed trains of 1 ms pulses at 10 pulse/s rate. **(E)** Example broadband recording during a pulse train containing 1 ms pulses at 10 pulse/s rate; optogenetic stimulation (blue). Inset: Response to a single pulse. **(F)** Example multiunit filtered data from (D). *Inset*: Stimulation-elicited spike.

Figure 4. Neuronal dynamics driven by optogenetic stimulation at an example site. (A) Neuronal responses to 5 ms pulse duration, 20 Hz pulse rate, periodic pulse train. (i) raster (top) and PSTH (bottom) of the response to single light pulses (blue). (ii) Mean evoked potential for all the stimulation pulses that were the last in a sequence and not preceded by a prior stimulation pulse within 50 ms, normalized by subtracting the value of LFP activity at the onset of the light. Dotted line indicates 0 mV. (iii) Spike-field coherence for multi-unit activity and LFP measured on the same electrode. (iv) Power spectral density (PSD) of 1 s of data during stimulation (black line) and spontaneous activity prior to stimulation (grey line). The dotted lines are error bars determined by the Chi-squared test for p=0.01. Solid gray lines above the PSD illustrate frequency bands where the stimulus PSD was significantly different from the spontaneous PSD ($p<0.01$). (v) Power spectral ratio showing frequency specific increases in power due to stimulation. (vi) Time-frequency spectrogram normalized by dividing the PSD of the spontaneous activity. **(B)** Same as (A) for 20 ms, 20 pulses/s pulse rate, Poisson pulse train. **(C)** SFC for 5 ms, 10 ms, 15 ms, and 20 ms pulse durations (20 pulses/s rate) averaged across all sites with driven multi-unit activity for the three subjects. **(D)** Normalized PSR for 2 ms, 5 ms, 8 ms, 10 ms, 12 ms, 15 ms, 18 ms, and 20 ms (20 pulses/s rate) averaged across all sites with

driven LFPs for the three subjects. **(E)** Mean frequency of peaks for the SFC (red) and PSR (black) for each pulse duration across all subjects. The mean SFC peak location was measured from the average SFC across all animals. The PSR peak location was measured individually for each recording site then averaged. Error bars show the standard error of the mean.

Figure 5. Site specific E-I windows generate different dynamics. (A) Transfection patterns and network connectivity can vary within a single injection site or across injection sites or subjects. **(B)** At the example site from Fig. 3 (Site A) a 20 ms pulse drives a longer evoked response in LFP activity (*dotted gray*). This can be modelled as an E-I window (*black*) with excitatory (*blue*) and inhibitory (*red*) components that have extended durations. Using this E-I window in the model results in narrow band coherent dynamics at low frequencies. **(C)** Same as (B) for Site A, with a 5 ms wide pulse. **(D)** Same as (C) for a different site.

Figure 6. Excitation window model for mapping parameterization. (A) Example E-I window for a empirical data using a 10 ms pulse duration temporally scaled to simulate E-I windows for 5 ms (*blue*), 20 ms (*green*), and 50 ms (*purple*) pulses. **(B)** *Top*, Simulated PSRs for 2-50ms pulses using an example excitation window from the 10 ms condition. Black dots show the actual PSR peak location from the experimental data. *Bottom*, same as top plotted on linear frequency scale. **(C)** *Top row*, PSRs for simulated responses in (B) for 5 ms, 10 ms, 20 ms, and 50 ms pulse duration conditions. *Bottom row*, same as top row plotted on linear frequency scale. Lighter, thinner lines show PSRs for experimental data.

Figure 7. Excitation window model predictions for quasi-periodic stimulation

(A) Quasi-periodic stimulation to generate stimulation pulses according to probability $P(stim) = \beta(1+\alpha\sin(2\pi Ft))\Delta t$. β is the baseline stimulation rate and α is the modulation depth of stimulation. F is the frequency of interest. Δt is the sampling rate of the simulation pulse train.

Increasing α increases stimulation intensity at frequency F. **(B)** Predicted PSR for fully periodic stimulation (F = 35 Hz) with 15 ms evoked potentials. *Inset*, Linear model prediction. **(C)** Predicted PSR for quasi-periodic stimulation (F = 35 pulse/s, α = 20, β = 5). **(D)** Trial-by-trial PSRs for the simulated responses from (C). **(E)** Responses when varying modulation depth α. Other parameters as in C. **(F)** Responses when varying frequency F. Other parameters as in (C). **(G)** Predicted responses using evoked potentials from 2 ms pulses for F = 65 Hz (*red*) compared with results from (C) (*blue*).

Figure 1

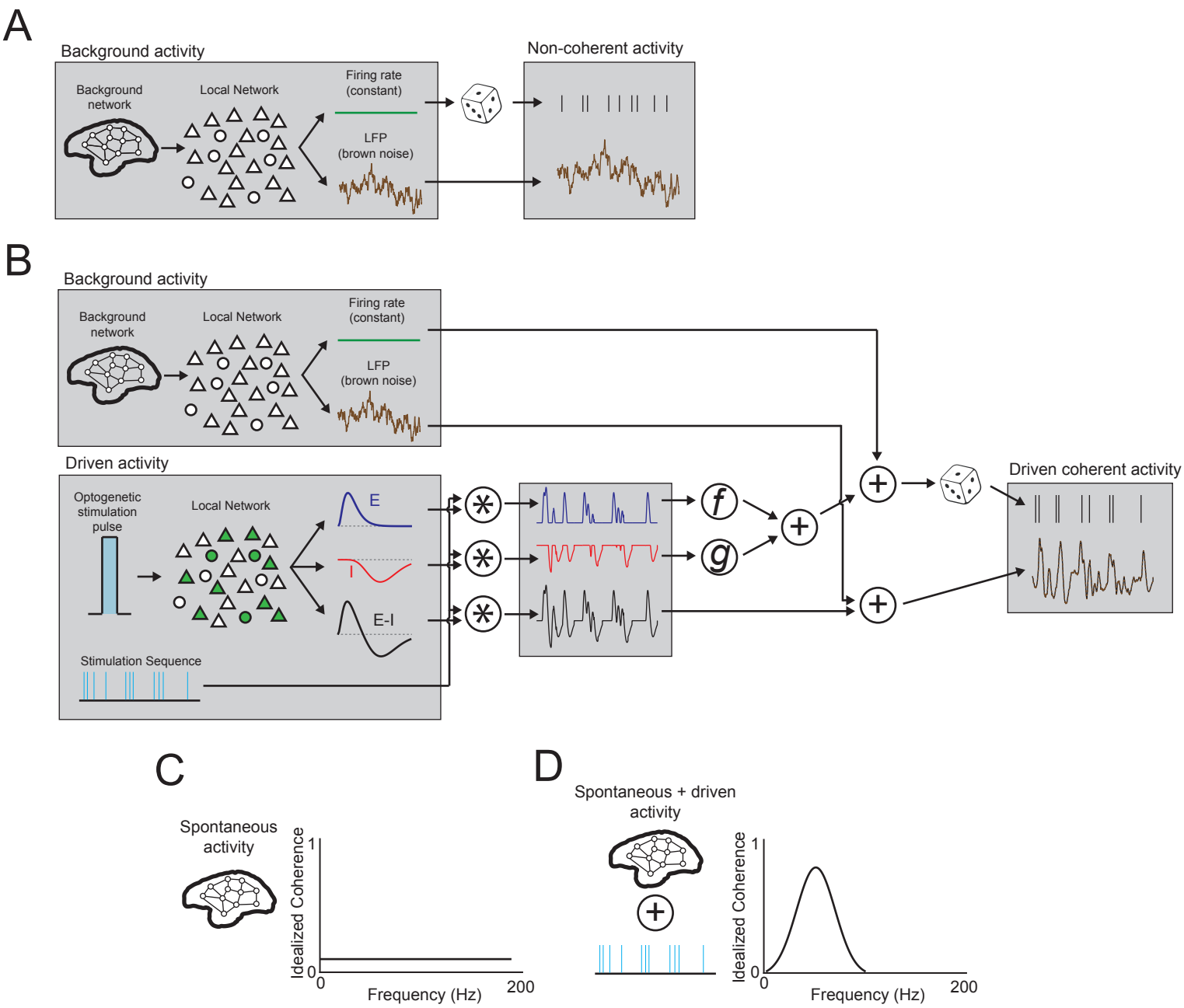

Figure 1. Excitation and inhibition drive coherent neuronal dynamics. (A) During spontaneous activity, synaptic inputs driven activity in a local network. We model spiking as being generated from a Poisson process with a constant rate and LFP as being generated from a Brown noise process. Under these assumptions, spontaneous spiking is not coherent with spontaneous LFP. **(B)** To model of optogenetic stimulation of a transfected, we simulated pulsatile responses generated by direct activation of ChR2 channels and synaptic activity. Pulsatile responses are convolved with a stimulation sequence. The summed excitatory and inhibitory (E-I, black) components comprise the simulated LFP. The individual E (blue) and I (red) windows, govern the variable spiking rate in the Poisson process which generates coherent spiking. **(C)** Spontaneous activity in the model has no spike-field coherence. **(D)** Optogenetic stimulation drives correlated fields and spiking, leading to frequency selective spike-field coherence.

Figure 2

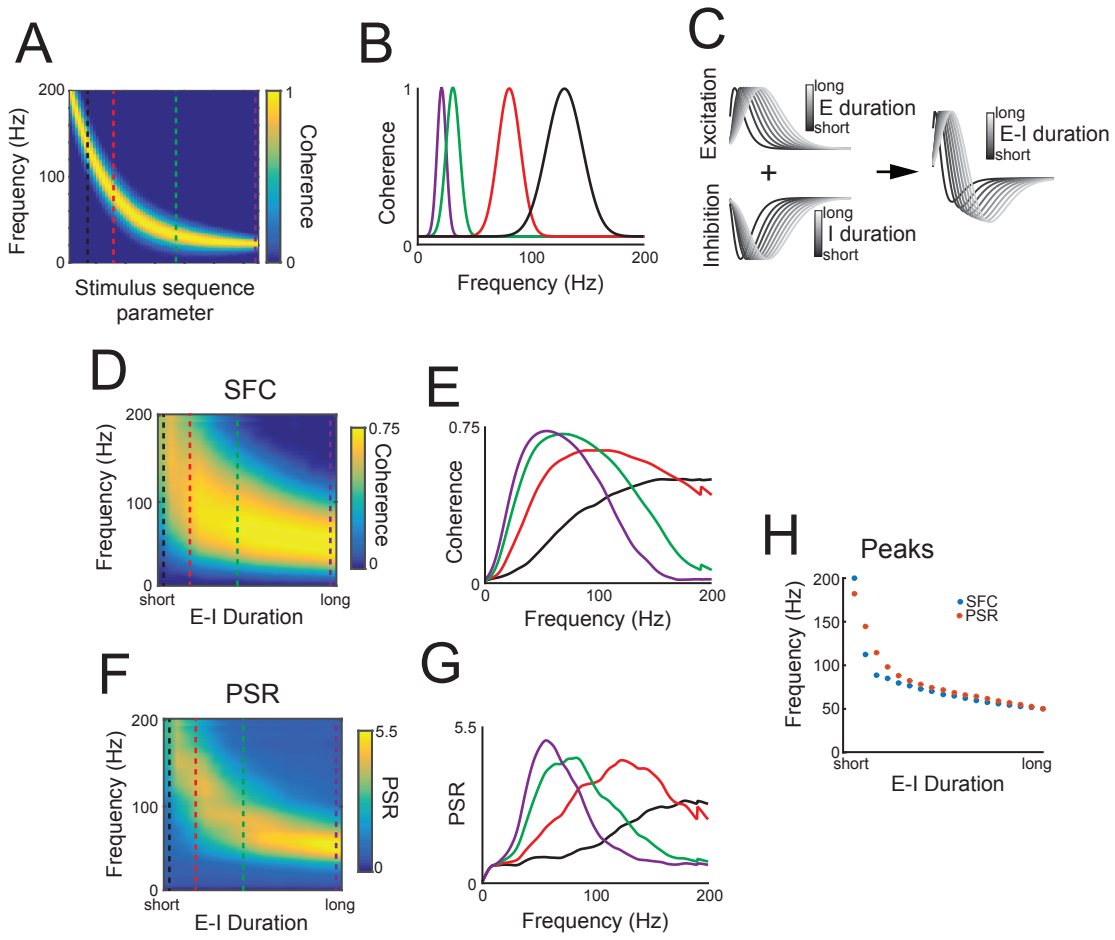

Figure 2. E-I window shape controls frequency of coherent activity. (A) Idealized generation of frequency selective coherent neuronal dynamics. The frequency content of the coherent activity varies with stimulation parameters. **(B)** Example coherence for various stimulus parameters in (A). **(C)** Excitation, inhibition and E-I windows with varying parameters to alter the duration of the windows. E-I is the sum of E and I windows. **(D)** Spike-field coherence that results from using the E-I windows from (C) in the model. **(E)** Example coherence for various E-I durations in (D). **(F)** Power spectral ratio that results from using the E-I windows from (C) in the model. **(G)** Example PSRs for various E-I durations in (F). **(H)** Right, frequency of peaks in the SFC (blue) and PSR (red) for each E-I window duration.

Figure 3

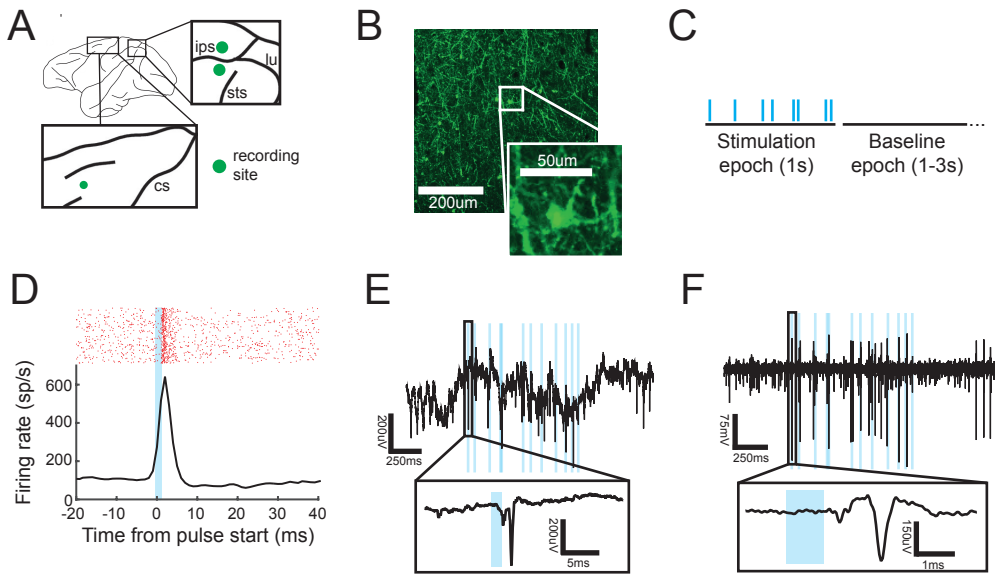

Figure 3. Optogenetic stimulation in macaque cortex. (A) Recording locations in all animals. The area of the circle corresponds to the number of sites recorded in each animal. **(B)** Example injection site with YFP labeled neurons and neuropil from horizontal section. Inset: image of a single transduced neuron. **(C)** Experimental design featured a 1 s stimulation pulse sequence followed by 1-3 s without stimulation. **(D)** Example raster plot (top) and PSTH (bottom) of the spiking response triggered on each stimulation pulse for Poisson distributed trains of 1 ms pulses at 10 pulse/s rate. **(E)** Example broadband recording during a pulse train containing 1 ms pulses at 10 pulse/s rate; optogenetic stimulation (blue). Inset: Response to a single pulse. **(F)** Example multiunit filtered data from (D). Inset: Stimulation-elicited spike.

Figure 4

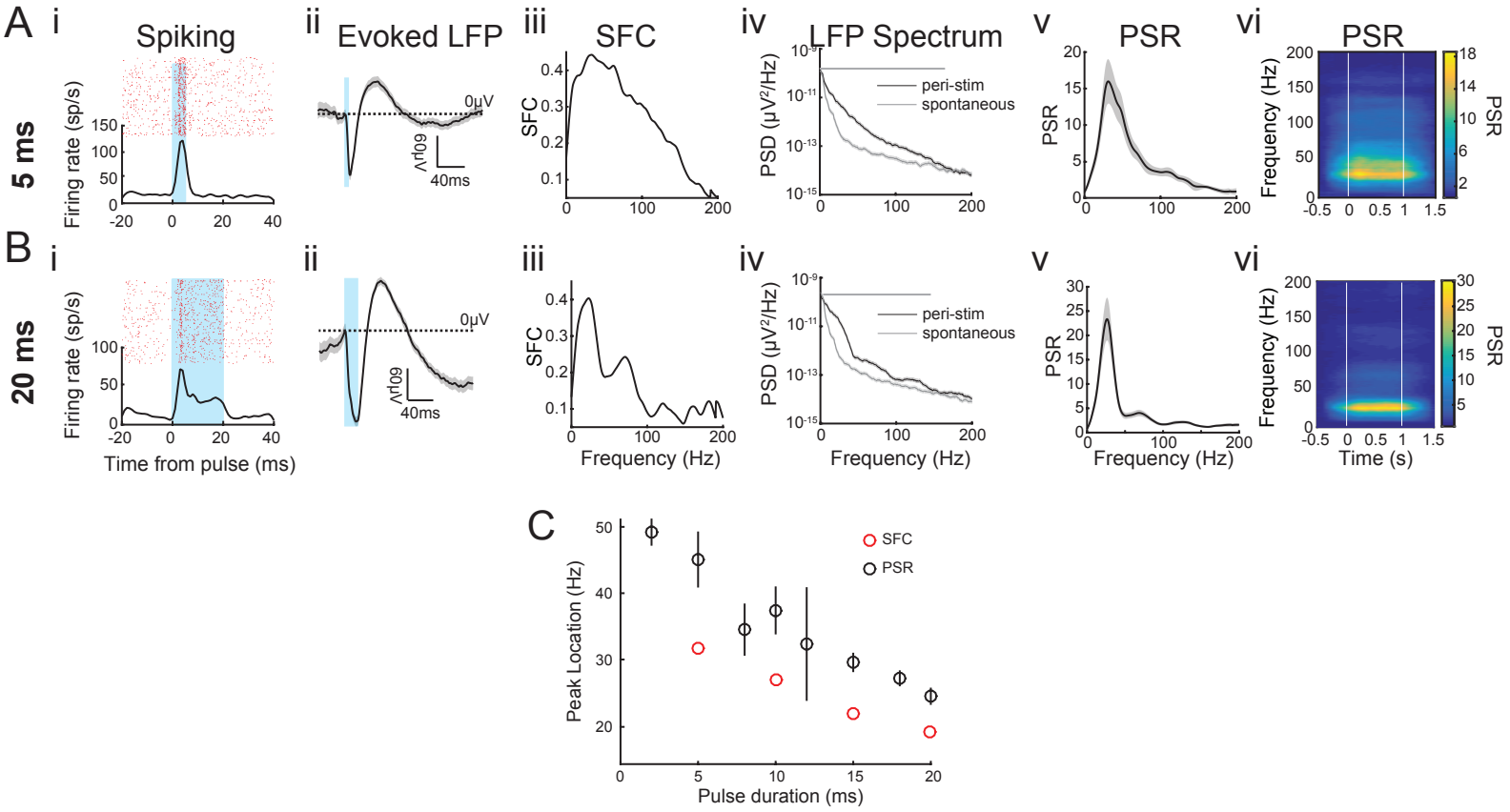

Figure 4. Neuronal dynamics driven by optogenetic stimulation at an example site. (A) Neuronal responses to 5 ms pulse duration, 20 Hz pulse rate, periodic pulse train. (i) raster (top) and PSTH (bottom) of the response to single light pulses (blue). (ii) Mean evoked potential for all the stimulation pulses that were the last in a sequence and not preceded by a prior stimulation pulse within 50 ms, normalized by subtracting the value of the LFP at the onset of the light. Dotted line indicates 0 mV. (iii) Spike-field coherence for multi-unit activity and LFP measured on the same electrode. (iv) Power spectral density (PSD) of 1 s of data during stimulation (black line) and spontaneous activity prior to stimulation (grey line). The dotted lines are error bars determined by the Chi-squared test for p=0.01. Solid gray lines above the PSD illustrate frequency bands where the stimulus PSD was significantly different from the spontaneous PSD (p<0.01). (v) Power spectral ratio showing frequency specific increases in power due to stimulation. (vi) Time-frequency spectrogram normalized by dividing the PSD of the spontaneous activity. **(B)** Same as (A) for 20 ms, 20 pulses/s pulse rate, Poisson pulse train. **(C)** Mean frequency of peaks for the SFC (red) and PSR (black) for each pulse duration across all subjects. The mean SFC peak location was measured from the average SFC across all animals. The PSR peak location was measured individually for each recording site then averaged. Error bars show the standard error of the mean.

Figure 5

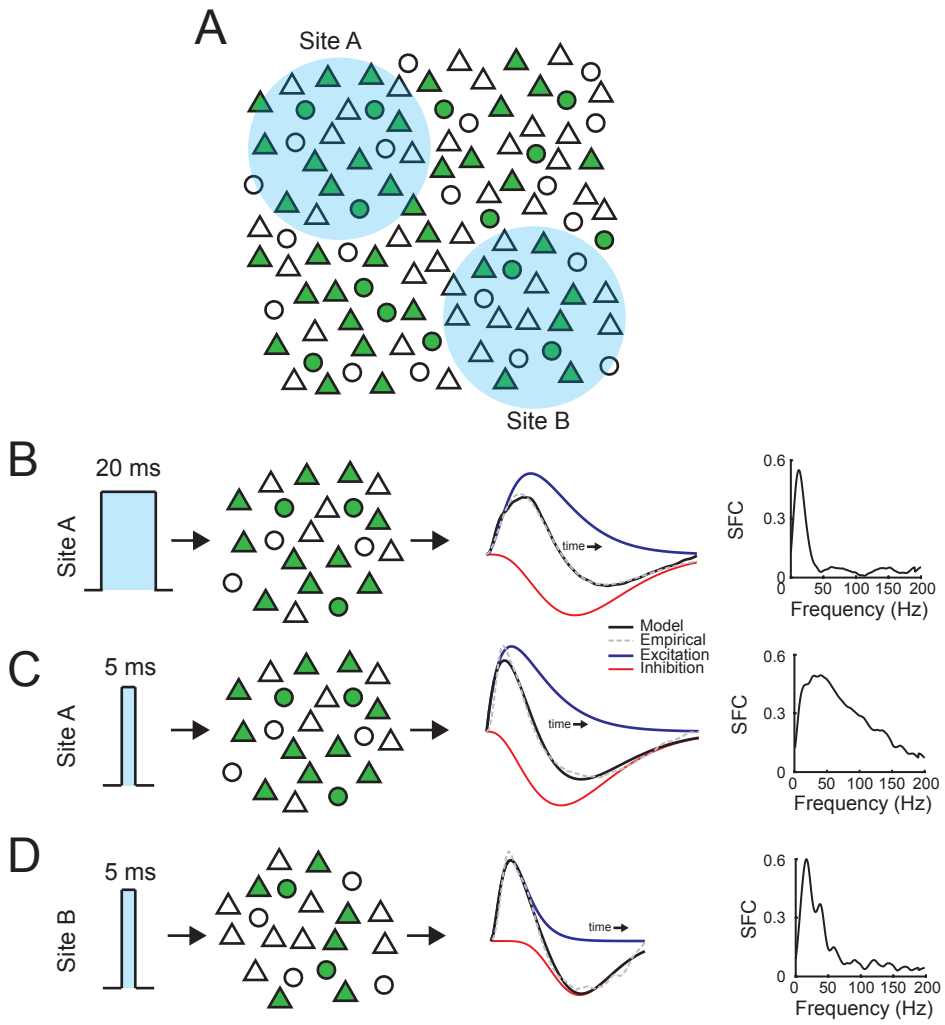

Figure 5. Site specific E-I windows generate different dynamics. (A) Transfection patterns and network connectivity can vary within a single injection site or across injection sites or subjects. **(B)** At the example site from Fig 3 (Site A) a 20 ms pulse drives a longer evoked response in the LFP (dotted gray). This can be modelled as an E-I window (black) with excitatory (blue) and inhibitory (red) components that have extended durations. Using this E-I window in the model results in narrow band coherent dynamics at low frequencies. **(C)** Same as (B) for Site A, with a 5 ms wide pulse. **(D)** Same as (C) for a different site.

Figure 6

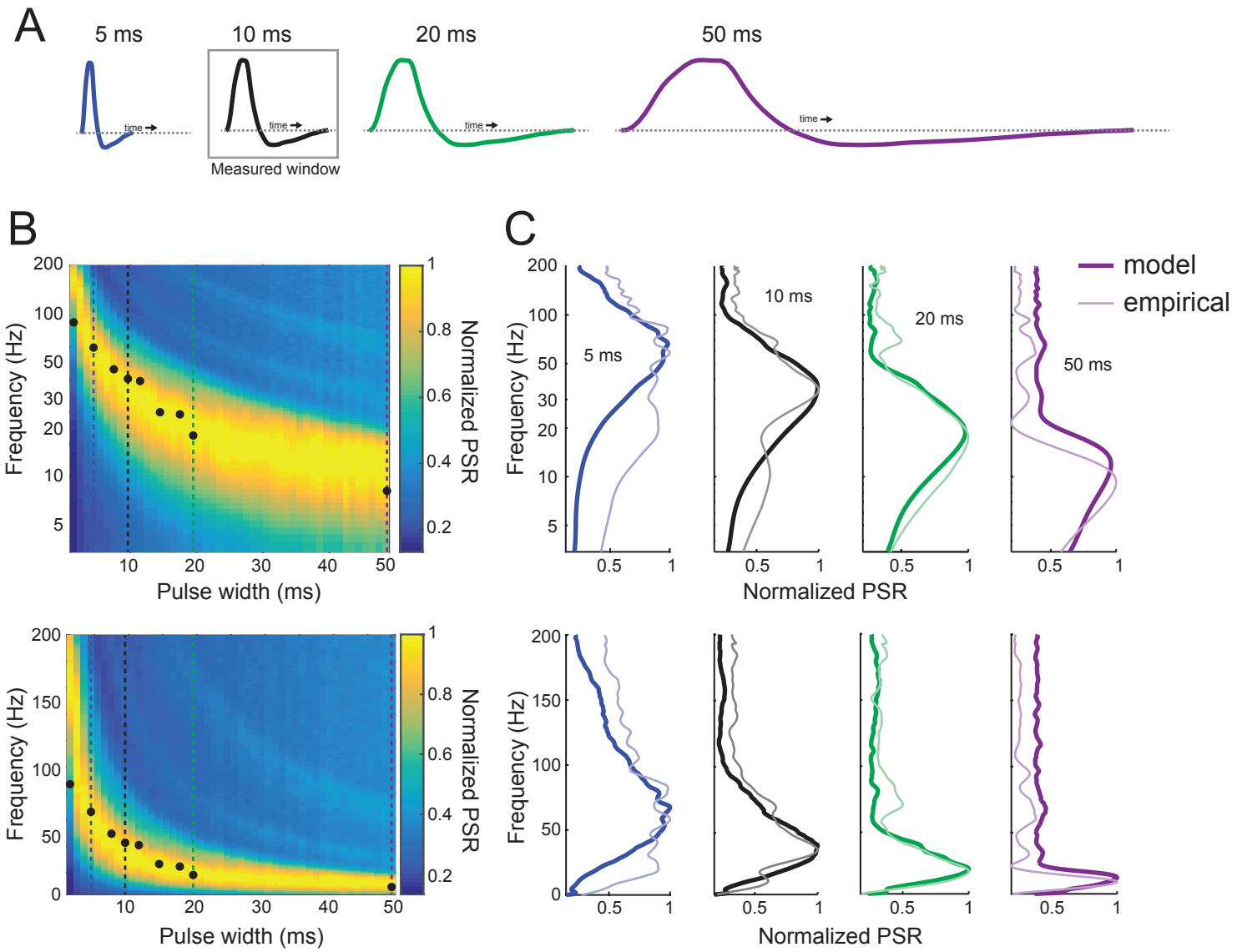

Figure 6. Excitation window model for mapping parameterization. (A) Example E-I window for a empirical data using a 10 ms pulse duration temporally scaled to simulate E-I windows for 5 ms (blue), 20 ms (green), and 50 ms (purple) pulses. **(B)** Top, Simulated PSRs for 2-50ms pulses using an example excitation window from the 10 ms condition. Black dots show the actual PSR peak location from the experimental data. Bottom, same as top plotted on linear frequency scale. **(C)** Top row, PSRs for simulated responses in (B) for 5 ms, 10 ms, 20 ms, and 50 ms pulse widths conditions. Bottom row, same as top row plotted on linear frequency scale. Lighter, thinner lines show PSRs for experimental data.

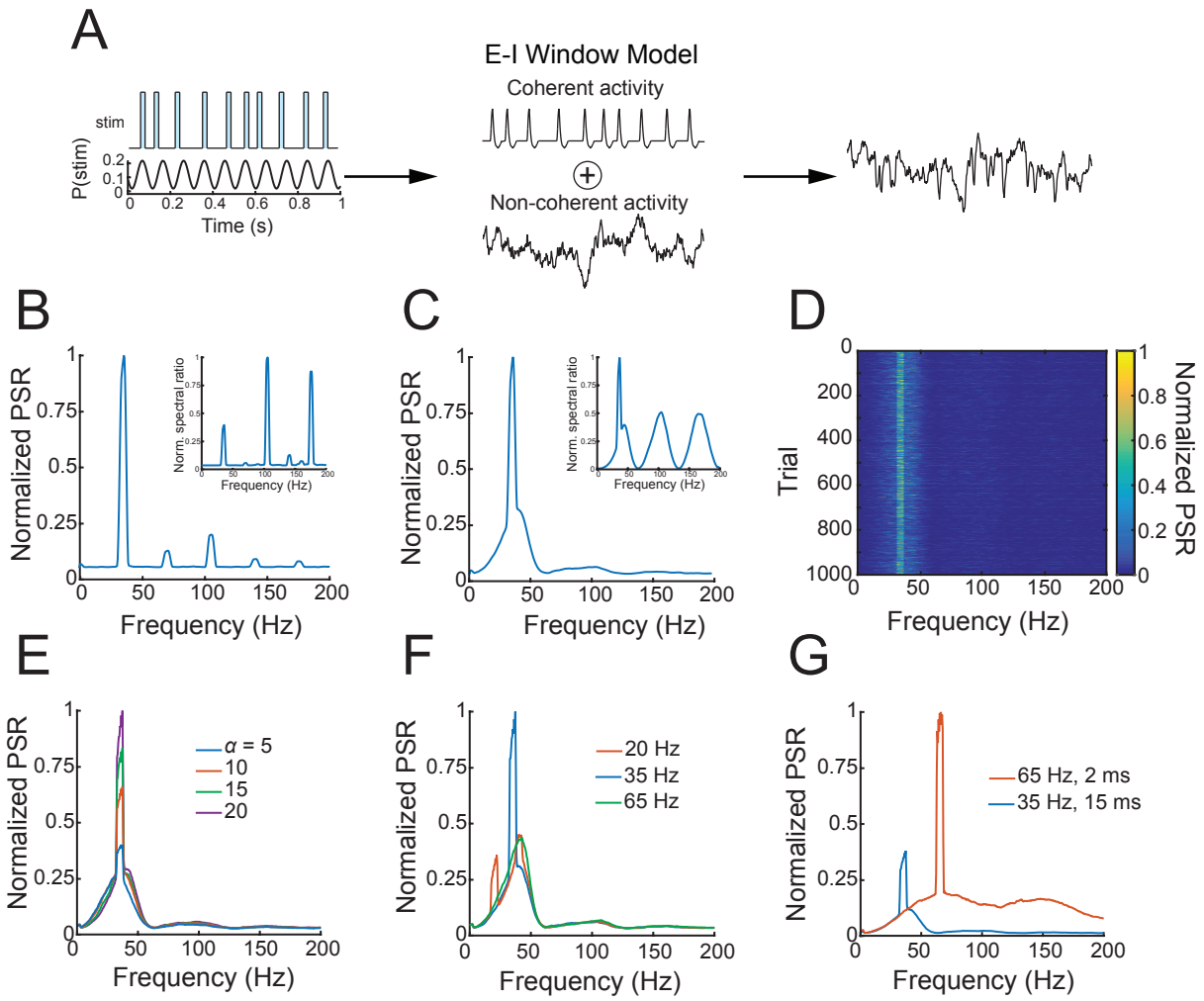

Figure 7. Excitation window model predictions for quasi-periodic stimulation. (A) Quasi-periodic stimulation to generate stimulation pulses according to probability P(stim) = β(1+αsin(2πFt))Δt. β is the baseline stimulation rate and α is the modulation depth of stimulation. F is the frequency of interest. is the sampling rate of the simulation pulse train. Increasing α increases stimulation intensity at frequency F. **(B)** Predicted PSR for fully periodic stimulation (F = 35 Hz) with 15 ms evoked potentials. Inset, Linear model prediction. **(C)** Predicted PSR for quasi-periodic stimulation (F = 35 pulse/s, α = 20, β = 5). **(D)** Trial-by-trial PSRs for the simulated responses from C. **(E)** Responses when varying modulation depth α. Other parameters as in C. **(F)** Responses when varying frequency F. Other parameters as in C. **(G)** Predicted responses using evoked potentials from 2 ms pulses for F = 65 Hz (red) compared with results from C (blue).